

## Key Points:

- The oblique ramps of the study area formed due to the oblique inversion of a rift related graben-system
- During inversion, those pre-existing normal faults were reactivated, that enclosed a high angle to the direction of shortening
- Spatial relationship of the inversion related oblique ramps and the earlier normal faults led us to define four styles of oblique inversion

## Correspondence to:

G. Héja,  
[hejagabor@hotmail.com](mailto:hejagabor@hotmail.com)

## Citation:




Héja, G., Ortner, H., Fodor, L., Németh, A., & Kövér, S. (2022). Modes of oblique inversion: A case study from the Cretaceous fold and thrust belt of the western Transdanubian Range (TR), West Hungary. *Tectonics*, 41, e2021TC006728. <https://doi.org/10.1029/2021TC006728>

Received 18 JAN 2021

Accepted 15 FEB 2022

© Wiley Periodicals LLC. The Authors. This is an open access article under the terms of the [Creative Commons Attribution License](https://creativecommons.org/licenses/by/4.0/), which permits use, distribution and reproduction in any medium, provided the original work is properly cited.

## Modes of Oblique Inversion: A Case Study From the Cretaceous Fold and Thrust Belt of the Western Transdanubian Range (TR), West Hungary

G. Héja<sup>1,2</sup> , H. Ortner<sup>3</sup> , L. Fodor<sup>2,4</sup> , A. Németh<sup>5</sup>, and S. Kövér<sup>2,4</sup>

<sup>1</sup>Mining and Geological Survey of Hungary, Budapest, Hungary, <sup>2</sup>Department of Geology, Institute of Geography and Earth Sciences, Eötvös University, Budapest, Hungary, <sup>3</sup>Institute of Geology, University of Innsbruck, Innsbruck, Austria, <sup>4</sup>MTA-ELTE Geological, Geophysical and Space Science Research Group of the Hungarian Academy of Sciences at Eötvös University, Budapest, Hungary, <sup>5</sup>MOL Hungarian Oil and Gas Plc., Budapest, Hungary

**Abstract** Inversion of pre-existing normal faults is a frequent phenomenon in orogenic belts. However, their impact on the evolution of the Cretaceous Eoalpine orogeny is poorly studied, despite the widespread presence of Triassic and Jurassic normal faults. Our study area is the SW part of the Transdanubian Range (TR), which represents the uppermost thick-skinned nappe of the Eoalpine orogeny in the Alpine realm. The variable trend of Cretaceous contractional structures within the Transdanubian Range has been traditionally explained by poly-phase shortening. However, based on the combined analyses of field observations and 3D seismic data, we found that the complex geometry of Cretaceous contractional structures can be explained rather by the oblique inversion of segmented Late Triassic grabens. In general, the SW part of the TR can be characterized by N-S trending contractional structures. NW-SE striking oblique ramps are nucleated above Late Triassic normal faults, whereas NE-SW trending folds and thrust with limited strike-parallel length evolved due to the inversion of pre-existing breached relay ramps, which connected the segments of Late Triassic normal faults. We determined different types of oblique ramps, including normal faults, which suffered transpressional reactivation, oblique hanging wall breakthrough thrusts, oblique footwall short-cut and hanging wall by-pass thrusts. Only very steep normal faults, or those that strike at low angle to the regional E-W shortening direction, were not reactivated.

### 1. Introduction

The presence of multidirectional folds and thrusts is widespread in fold and thrust belts, although their origin is not always clear. In several cases multidirectional contractional structures are explained as a result of temporally distinct phases of shortening. A nice example for that is the eastern part of the Southern Alps, where SE vergent Paleogene Dinaric thrusts are overprinted by south-vergent Neogene Alpine thrusts (Doglioni, 1987) causing Type 1 re-fold patterns (Ramsay, 1967). In other cases oblique and lateral folds and thrusts form due to differential displacement above a thrust or decollement (displacement gradient; e.g., Marshak et al., 1992; Muñoz et al., 2013), or tectonic transport above an oblique/lateral ramp (e.g., Apotria et al., 1992). In numerous cases structural inheritance of pre-existing normal faults is responsible for the formation of oblique/lateral ramps. Oblique inversion of pre-existing extensional grabens, which strike non-parallel to the orogen, have been described from several fold-and-thrust belts (e.g., Iberian Chain, De Vicente et al., 2009; Jura Mountains, Ustaszewski & Schmid, 2006; Betic Cordillera, Pedrera et al., 2020; Atlas, Beauchamp et al., 1996). Oblique graben inversion has been studied in numerous analogue (Amilibia et al., 2005, 2008; Brun & Nalpas, 1996; Deng et al., 2019; Granado et al., 2017; Marques & Nogueira, 2008; Sassi et al., 1993; Yagupsky et al., 2008) and numerical models (Ruh, 2019), as well.

We study the western part of the Transdanubian Range (TR) of Hungary (Figure 1a), which represents the uppermost unit (Figure 1b) of the Cretaceous nappe stack of the Eastern Alps (Austroalpine nappe stack formed during the Eoalpine orogeny; Schmid et al., 2008). The multidirectional folds and thrusts of the TR have traditionally been explained at least by two or even three temporally distinct phases of shortening during the long-lasting Cretaceous orogeny (Pocsai & Csontos, 2006; Sasvári, 2008, 2009; Tari, 1994; Tari & Horváth, 2010). Although, the presence of Triassic and Jurassic pre-orogenic normal faults has been known for a long time (e.g., Budai & Vörös, 2006; Héja et al., 2018; Vörös & Galács, 1998), their possible effect on the Cretaceous shortening has not yet been investigated. In this study, we focus on the role of inherited Triassic normal faults on subsequent Cretaceous folding, and investigate whether differences in fold trend have any connection to pre-existing normal

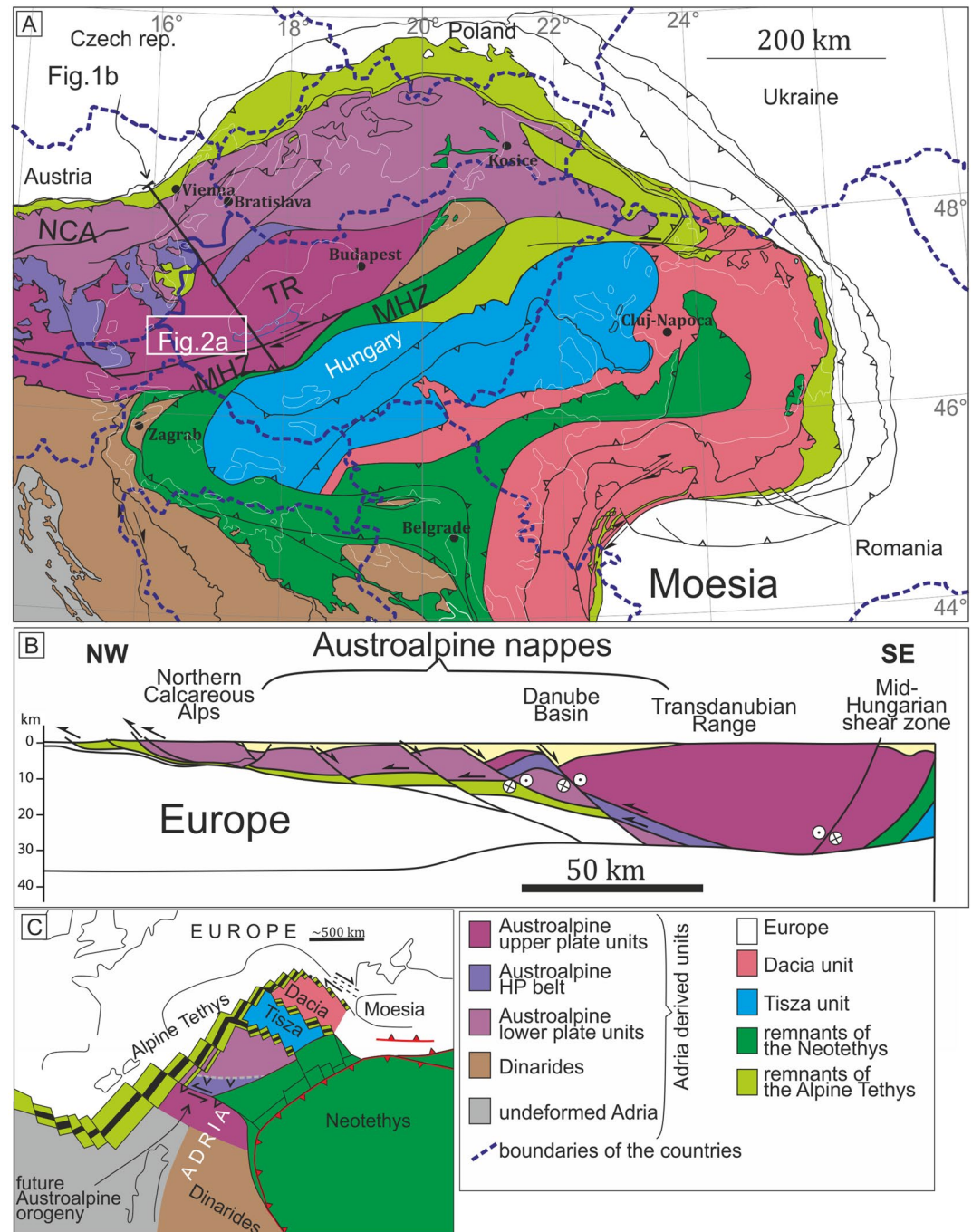


**Figure 1.** (a) Tectonic units of the Alpine collision zone (Schmid et al., 2020, modified); NCA = Northern Calcareous Alps, TR = Transdanubian Range, MHZ = Mid-Hungarian Shear Zone. White line indicates the surface exposure of the pre-Miocene basement; (b) Crustal-scale profile across the easternmost Alps and the western Pannonian basin (study area) (Schmid et al., 2020; Tari, 1994, modified) (c) Position of the Austroalpine units on the Adriatic plate during the Late Jurassic (Schmid et al., 2008, modified).

faults. Our conclusions are based on surface observations from the Keszthely Hills (KH; Figures 2a and 2b; Héja et al., 2022) and the interpretation of a 3D seismic data set in the adjacent Zala Basin (Figures 2a and 2b); the two types of datasets depict various aspects of the same pre-orogenic fault system and its inversion.

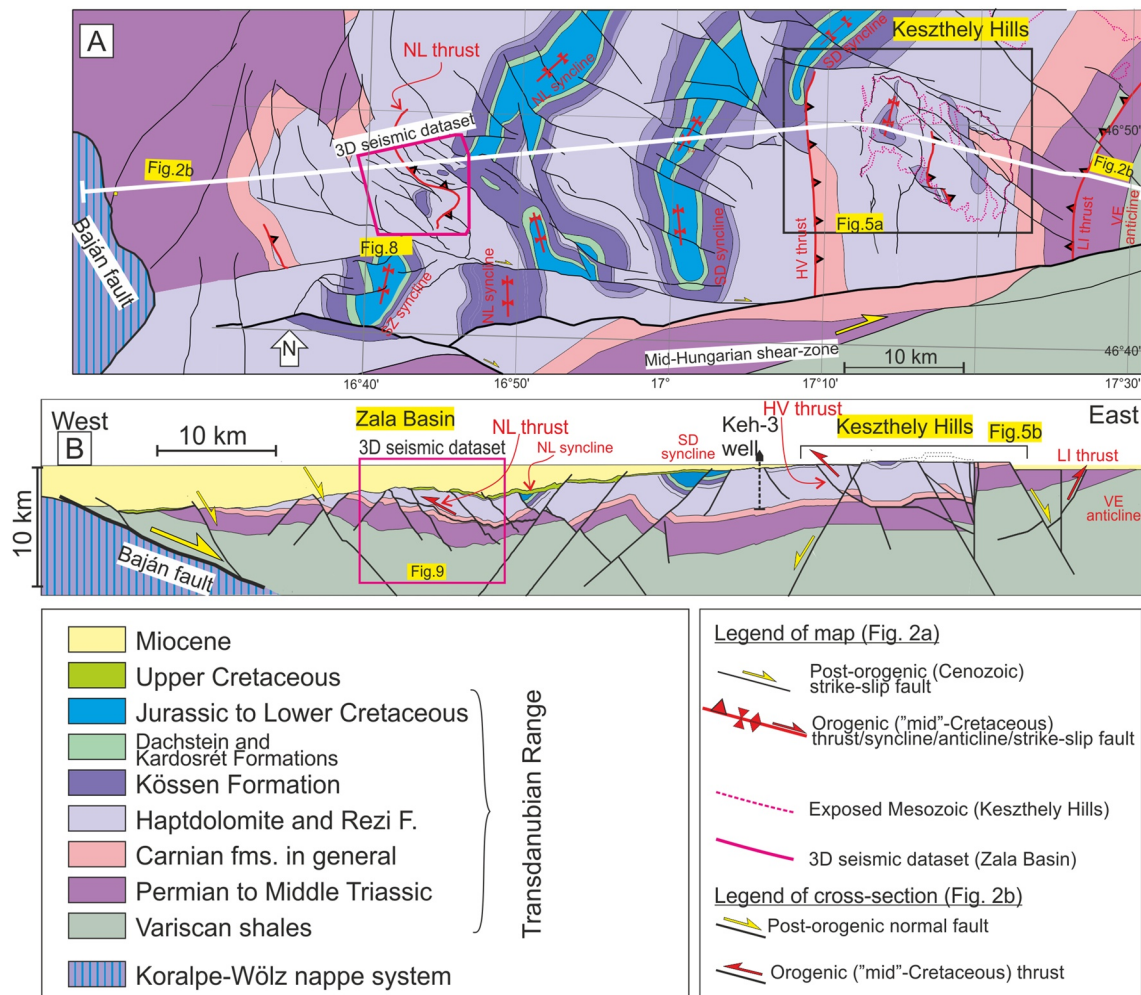


**Figure 2.** (a) Subcrop map of the folded Mesozoic at the level of the base-Upper Cretaceous in the western TR and Zala Basin (after Fodor et al., 2013, modified); for location of the map see Figure 1a; (b) Location of the 3D seismic data set and the Keszthely Hills on a regional cross-section (after Fodor et al., 2021, modified); for location of the section see panel (a) Location of the 3D seismic block is indicated by red rectangle; the Keszthely Hills is indicated by a black rectangle.

## 2. Geology of the Study Area

The Transdanubian Range (TR) is built up by Variscan low-grade metamorphic rocks and Permian to Cenozoic non-metamorphic succession. Being a part of the Austroalpine nappe system (Figures 1a and 1b), the post-Variscan deformation and basin evolution of the TR was dependent on the opening and closure of two oceanic basins: the Neotethys in the east, and the Alpine Tethys in the northwest (Figure 1c; Haas et al., 1995; Handy et al., 2010; Schmid et al., 2008).

Deposition of the Permian continental siliciclastic sediments and Lower to Middle Triassic shallow marine mixed carbonate-siliciclastic beds (Figure 3) was controlled by the continental rifting of the Neotethys (Haas et al., 1995). The onset of oceanic spreading of the Neotethys was followed by the post-rift subsidence of the Adriatic passive margin (including the TR) during Late Anisian to Late Triassic. Due to this subsidence, platforms and intraplatform basins formed during Late Anisian—Ladinian (Budai & Vörös, 2006). The intraplatform basins were filled up by deep marine marls during the Carnian (Figure 3; Haas et al., 2012). The Carnian basinal formations are laterally interfingering with a coeval carbonate platform, which was partly dolomitized in the eastern Keszthely Hills (Csillag et al., 1995). The deposition of the Hauptdolomit Formation (Figure 3) took place during Late Carnian to Norian in a back-reef lagoon environment. This formation is a thick-bedded bituminous dolomite with occasional stromatolite intercalations in the study area (Haas et al., 2012).



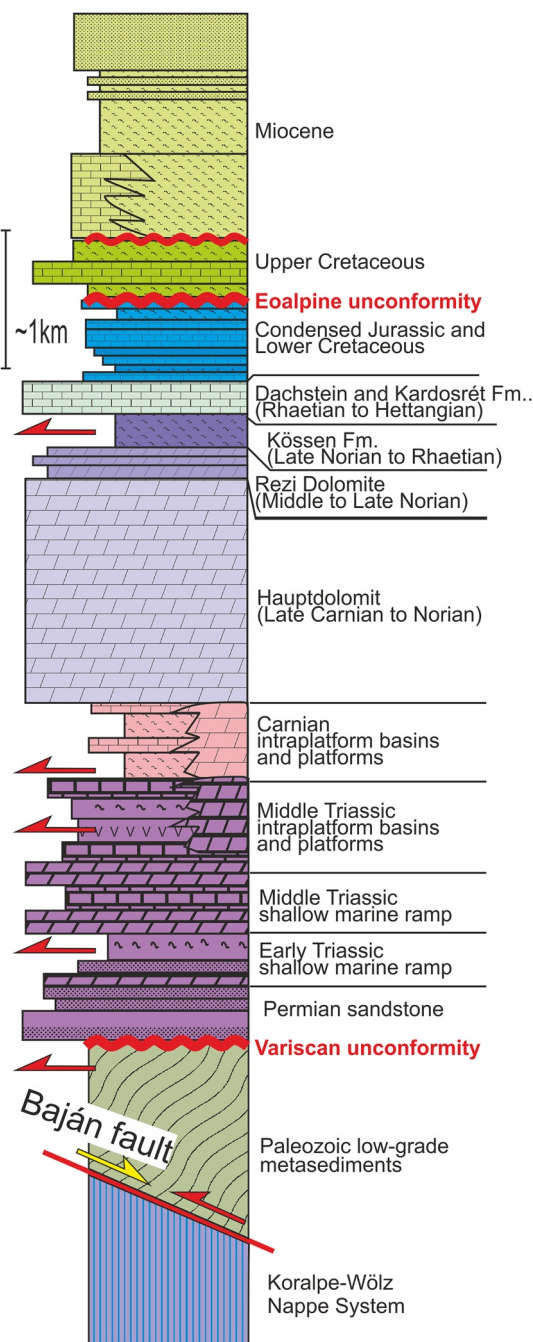


**Figure 3.** Stratigraphy of the study area. Red arrows show the most important decollement levels based on Linzer and Tari (2012).

Another pulse of extension reached the Austroalpine units during the latest Triassic—Middle Jurassic as a result of the incipient continental rifting of the Alpine Tethys (Figure 1c). This event was well pronounced in the western TR, and did cause significant extension (Csillag et al., 1995; Haas et al., 1995; Héja et al., 2018). The syn-rift deposits of this event are the Middle to Late Norian Rezi Dolomite—which is an alternation of dark-gray, cherty, bituminous, laminated dolomite and thick-bedded dolomite—and the Rhaetian Kössen Formation, which is made up by the alternation of dark-gray to black marl with high organic matter content and thin-bedded limestone intercalations (Figure 3; Budai & Koloszar, 1987). The Kössen Marl is overlain by the shallow marine Dachstein Limestone. The covering Jurassic succession of the TR can be characterized by condensed pelagic rocks, which were deposited on a submarine swell (Vörös & Galacz, 1998). From the Hauterivian to the Aptian deep-marine marls and an Aptian–Early Albian shallow marine limestone were deposited (Figure 3; Haas et al., 1984).

Middle Jurassic spreading of the Alpine Tethys can be connected to the onset of intra-oceanic subduction within the Neotethys (e.g., Handy et al., 2010). The closure of the Neotethys ocean remained active during the Early Cretaceous, which finally led to the formation of the Austroalpine nappe system during the middle Cretaceous (Eoalpine deformation; Figures 1b and 1c). The TR occupied the position of the uppermost thick-skinned nappe within the Austroalpine nappe system (Figure 1b) (Schmid et al., 2008; Tari, 1994). The TR suffered intense shortening related to this event. Several Eoalpine thrusts verging toward W or WSW, were interpreted in the Mesozoic basement of the Zala Basin by Tari (1994), Tari and Horváth (2010), Linzer and Tari (2012) and Fodor et al. (2013). The Jurassic to Lower Cretaceous deposits are preserved only in the core of major synclines in the Zala Basin (Figures 2a and 2b), and they are unconformably overlain by Upper Cretaceous (Senonian) deposits (Figures 2b and 3; Kőrössi, 1988). From west to the east these N-S trending major synclines are the SZ (Szilvágy) syncline, the NL (Nagylyngyel) syncline and the SD (Sümege-Devecser) syncline (Figures 2a and 2b).

Due to the ongoing convergence between Africa and Europe the Austroalpine nappes decoupled from their mantle lithosphere, which resulted in the onset of subduction of the Alpine Tethys during Late Cretaceous (Handy et al., 2010). Consumption of the Alpine Tethys led to the collision between Europe and Adriatic plate during the Late Paleogene (Figure 1b; Handy et al., 2010; Schmid et al., 2008). The slab of the Alpine Tethys started to tear below the Eastern Alps after collision, therefore slab-pull retreated under the Carpathians (Handy et al., 2010). Slab tear below the Eastern Alps in combination with the slab roll-back below the Carpathians resulted in the eastward lateral extrusion of a part of the Austroalpine nappes and the formation of the Pannonian back-arc basin during the Miocene (Figures 1a and 1b; Horváth et al., 2015; Ratschbacher et al., 1991; Royden, 1993). The Mid-Hungarian Shear Zone, which is running immediately south of the study area, represents an important dextral shear zone related to extrusion tectonics (Figure 1a). In

this WSW-ENE striking zone (Figure 2a) intense post-Eocene transpressional deformation occurred (Csontos & Nagymarosy, 1998; Fodor et al., 2013). The Zala Basin can be considered as one of the sub-basins of the Pannonian back-arc basin system (Fodor et al., 2013, 2021). The formation of the Zala Basin was controlled by the Baján low angle normal fault (Figures 2a and 2b). The Miocene infill of the Zala Basin forms a wide asymmetric half graben, which is dissected by a number of minor Miocene normal faults. The Keszthely Hills are located at the eastern edge of this halfgraben, therefore the Mesozoic succession is exposed there from beneath the thin Miocene deposits (Figures 2a and 2b).

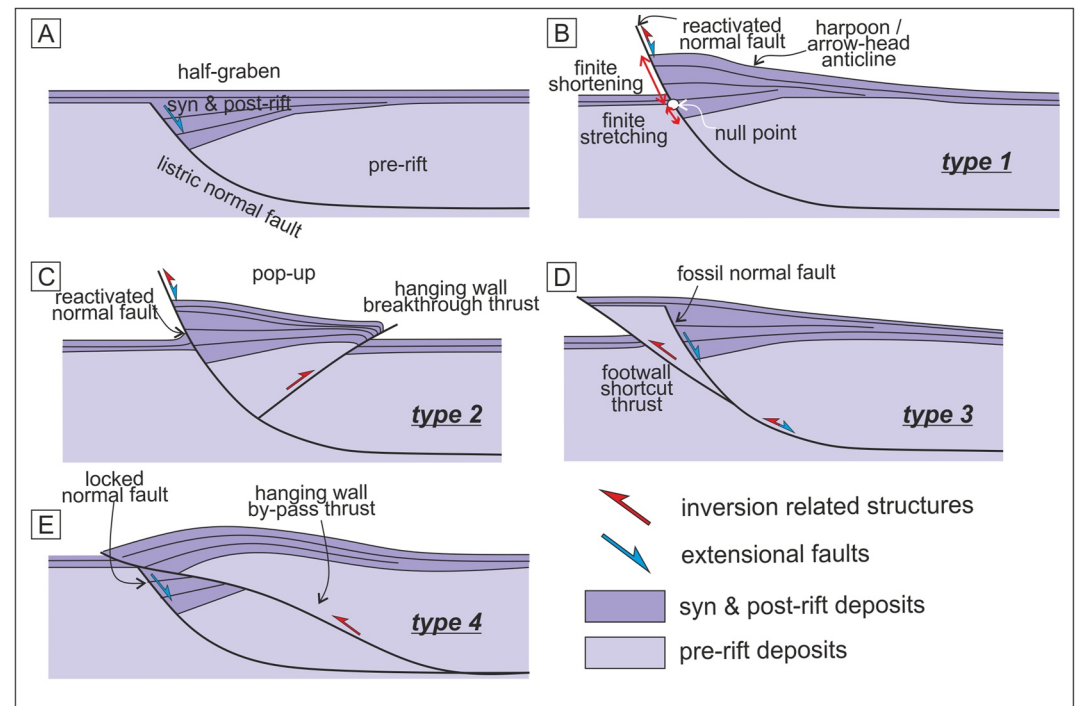


**Figure 4.** Types of inversion related structures. (a) Extensional roll-over above a listric normal fault prior to inversion. Light and dark purple colors represent pre-rift rocks and syn- and post-rift deposits, respectively; (b) inverted half-graben with harpoon/arrow-head anticline; (c) pop-up structure between a reactivated normal fault and a newly formed hanging wall breakthrough thrust; (d) footwall shortcut thrust; (e) hanging wall bypass thrust; references for figures are in the text; the end-member models of (b–e) are used for the classification of inversion related oblique ramps (see Figure 11).

### 3. Terminology of Inversion Tectonics

Inversion of pre-existing normal faults results in the formation of characteristic structures. The most frequent section-view geometries of inverted half-grabens are summarized in Figure 4. Identification of these inversion-related structures is crucial, in order to confirm the role of inversion in the formation of oblique contractional structures. Reactivation of the half graben bounding normal fault results in the uplift of the syn-rift sedimentary wedge, which often show characteristic “arrowhead” or “harpoon” geometry (Figure 4b; McClay, 1995). The amount of reactivation can be estimated based on the position of the null point which/that represents the point on the inverted normal fault, where a syn-rift marker horizon displaced by normal faulting regained its pre-inversion position during contractional reactivation (Williams et al., 1989). Marker horizons above and below the null point experience finite shortening, and finite stretching, respectively (Figure 4b; Williams et al., 1989). The null point progressively migrates downward during inversion, and the graben becomes totally inverted when the null point reaches the base of syn-rift strata.

Newly formed backthrusts in the hanging wall of reactivated normal faults are also frequent and termed hanging wall breakthrough thrusts (Figure 4c; Bonini et al., 2012). The extruded block between the reactivated normal fault and the hanging wall breakthrough thrust forms a pop-up (Figure 4c).

If the normal fault is locked during inversion, buttressing and/or newly formed thrusts accommodate shortening. Footwall shortcut thrusts cut across the footwall corner of the pre-existing normal fault. The pre-existing normal fault is frequently transported in the hanging wall of the shortcut thrust (Figure 4d; Bonini et al., 2012). Pre-existing normal faults frequently define the location of the footwall ramp of a thrust. In that case the pre-existing normal fault is by-passed by the thrust (hanging wall by-pass thrust on Figure 4e; McClay, 1995).

## 4. Methods and Data

We introduce a new structural interpretation of the Keszthely Hills, where the folded Triassic carbonates are found at the surface (Figures 2a and 2b). Our cross-sections and structural maps are based on the thorough structural study of the Triassic outcrops (Héja et al., 2022). These surface data provide useful analogies for the seismic interpretation of the 3D data set, which is located in the adjacent Zala Basin, where the folded Mesozoic rocks lie under a thick Upper Cretaceous and Cenozoic cover (Figures 2a and 2b).

The featured 3D seismic data set of the Zala Basin (Figures 8–10) was acquired in 2008–2010 mostly by vibroseis trucks. In areas that the thumper trucks could not reach, shallow boreholes were drilled with dynamite placed in them as an explosion source. Sweep frequency was 8–100 Hz. A coverage of 20 × 20 m bin size ensured that proper lateral resolution and a good signal/noise ratio was achieved even in the shallow parts. Both processing runs were normal PSTM workflows with minor differences in statics calculation (uphole based statics vs. GLI refraction statics) and noise attenuation. The strikes of IL and XL lines are 348°–168° and 78°–258°, respectively. The presented seismic sections (Figures 9 and 10) are arbitrary slices, section traces are shown on Figure 8.

The featured seismic sections of the 3D data set (Figures 9 and 10) of the Zala Basin are shown in the depth domain after a simplified time-depth conversion. The velocity model was calibrated based on correlation of the well tops depth and the depth of interpreted horizons in time. We were fitting data to the function of  $V = kz + V_0$ , in order to calculate the values of  $k$  and  $V_0$ , where  $V$  = velocity at a given depth;  $k$  = the rate of velocity change with depth;  $z$  = depth;  $V_0$  = initial velocity. Based on that, we calculated an initial velocity ( $V_0$ ) 2,360 m/s in the case of Miocene deposits, where the rate of velocity change with depth ( $k$ ) was 0.41. We used average values of velocities 3,860 and 6,250 m/s in the cases of Upper Cretaceous and Triassic-Jurassic rocks, respectively. The latter value is in accordance with the VSP data of Vorderib-1 (Northern Calcareous Alps) where the velocity of the Triassic succession (very similar to the Triassic of the TR) is range between 5 and 7 km/s (Dohr, 1981).

We constructed cross-sections across the Keszthely Hills, based on well and surface data (Figures 5b and 7). The thicknesses of the Carnian basinal formations and the Hauptdolomit are derived from seismic data of the north-western foreland of the Keszthely Hills (Héja et al., 2018).

## 5. Field and Seismic Examples of Oblique Inversion From the Southwestern Transdanubian Range

### 5.1. Oblique Inversion in the Keszthely Hills

#### 5.1.1. Pre-Existing Normal Faults of the Keszthely Hills

Late Triassic sedimentation of the Keszthely Hills (KH) took place in an asymmetric, WNW-ESE striking half-graben in the hanging wall of the CT (Cserszegtömaj) fault (Figure 5a), which came into being due to NNE-SSW extension (Héja et al., 2018). The syn-rift Rezi Dolomite preserved only in the hanging wall of this fault; the sedimentary breccia lithofacies of it—in the vicinity of the CT fault—suggests syn-sedimentary fault movement (Figure 6a; Csillag et al., 1995; Héja et al., 2018). The blocks of this breccia redeposited from shallow marine environment, which probably represented the footwall of the CT fault. Based on the map-view pattern, the CT fault is segmented; the overlapping NE-dipping segments are connected by relay ramps (Figures 5a and 6a). This segmented fault geometry is in accordance with the measured sedimentary transport directions, which were inferred from slump folds and slides (Héja et al., 2018, 2022). In general, sedimentary transport directions are pointing toward to the NE on the fault controlled slopes. However, transport directions turn toward to the E or SE on relay ramps (Héja et al., 2018, 2022). The R (Rezi) syncline is bounded by the western segment of the CT fault to the south. Its southward widening triangle shape (Figure 5a) was interpreted as a folded half-graben by Héja et al. (2018).

The exposed Carnian rocks—underlying the Hauptdolomit—are bounded by the NV (Nemesvita) fault to the north, the SM (Szent Miklós) fault to the west, and the ED (Ederics) fault from the southwest in the KH (Figure 5a). The age of these structures is more controversial, since there is no sign of syn-sedimentary faulting along these faults. Budai, Császár, et al. (1999) interpreted these structures as Cretaceous strike-slip faults. On the other hand, Héja et al. (2018) considered these faults as pre-orogenic normal faults based on the following facts. First of all, the SM fault is cut by a NW-SE striking tear-faults (description in the next section), which can



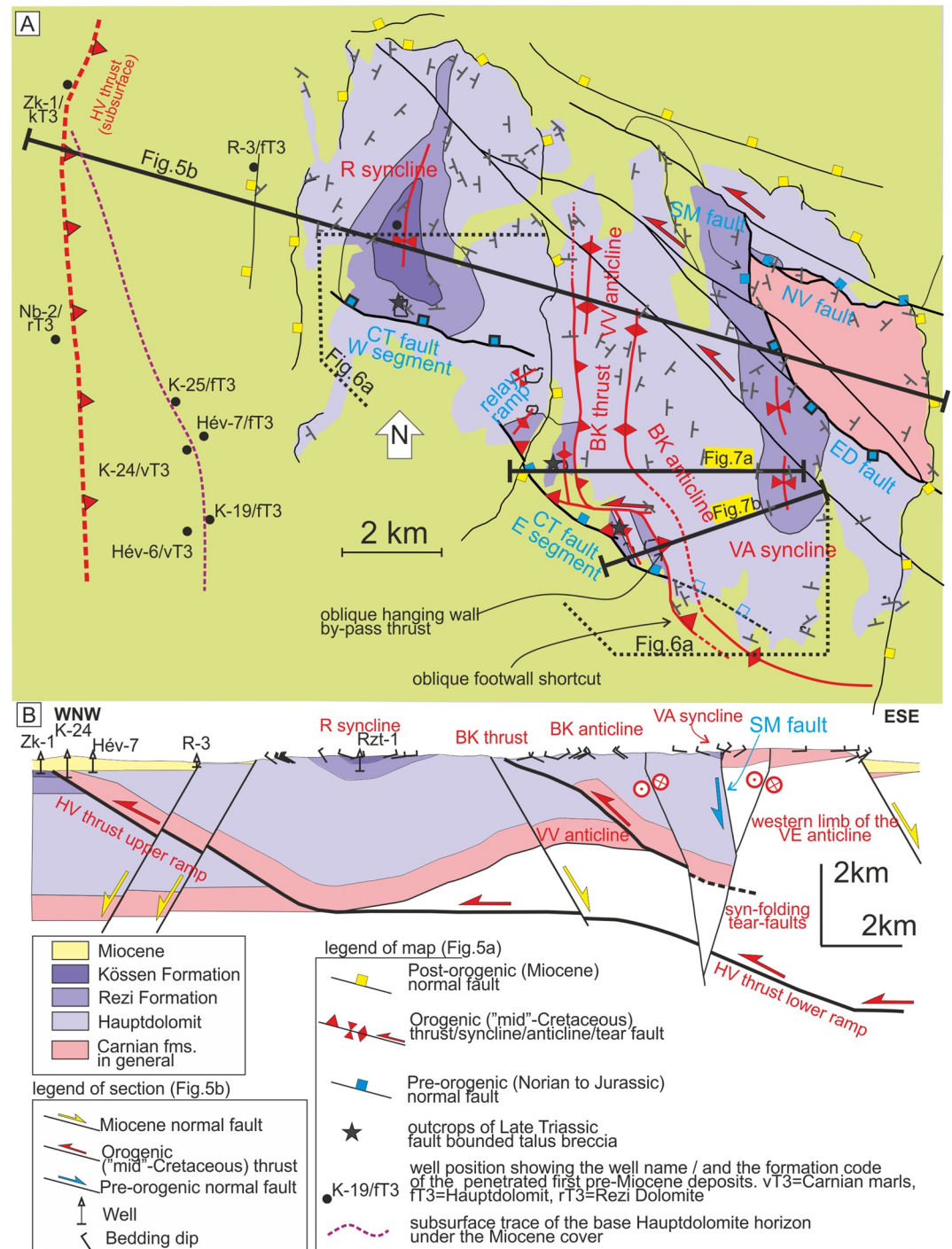


**Figure 5.** (a) Pre-Quaternary geological map of the Keszthely Hills based on Budai, Csillag, et al. (1999) and Héja et al. (2022) (for location of the map see Figure 2a); (b) WNW-ESE striking cross-section across the central Keszthely Hills (for location see panel a).

be interpreted as a Cretaceous syn-folding structures (Héja et al., 2018, 2022). This cross-cutting relationship suggests that the formation of the SM fault preceded shortening. Second, the approximate 60°–70° cut-off angle of the subvertical SM fault (based on electric sounding of Gulyás, 1991) and the west dipping Triassic beds of the surroundings rises the possibility that the SM fault is a pre-tilt or pre-folding normal fault (Figure 5b).

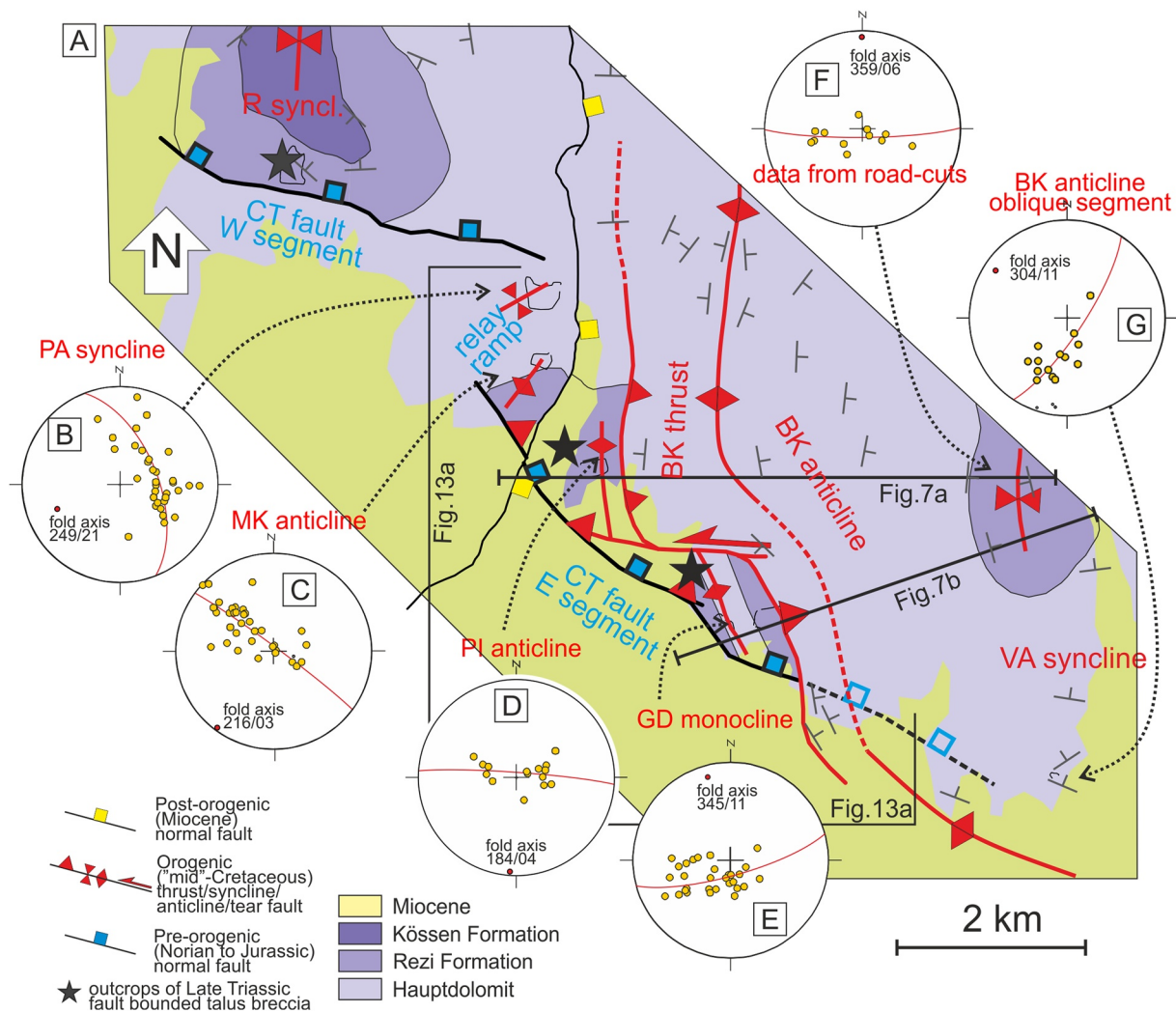


**Figure 6.** (a) Structural map of the southern Keszthely Hills, showing the segmented preorogenic CT fault, and the oblique inversion related folds and thrusts; (b–g) Stereoplots of the measured folds in different quarries (lower hemisphere, Schmidt net); poles to beds (yellow dots), best fitting great circle (red line) and calculated fold axes (red dot) are indicated.

### 5.1.2. Cretaceous Contractural Structures of the KH

The major compressional structures of the central and northern KH formed as a consequence of E-W shortening. The associated structures are represented by west directed thrusts—including the buried HV (Hévíz) thrust and the BK (Büdöskút) thrust—and several fault related folds with N-S trend: the R (Rezi) syncline, the VV (Várvölgy) anticline, the BK (Büdöskút) anticline and the VA (Vállus) syncline (Figure 5; Budai, Császár, et al., 1999; Budai, Csillag, et al., 1999; Fodor et al., 2013; Héja et al., 2022). Most of these structures are identified based on geological mapping (Budai, Csillag, et al., 1999; Héja et al., 2022). An exception is the Hévíz thrust, which is postulated by Fodor et al. (2013) based on wells in the western foreland of the KH (Figure 5a). The compressional structures of the KH are unconformably overlain by Miocene beds (Figure 5b), giving a poor time constraint for the age of contraction (Budai, Császár, et al., 1999). However, the presence of sub-horizontal Upper Cretaceous beds in the surrounding areas (e.g., Zala Basin) suggests that the folds of the KH are mid-Cretaceous structures, too (Fodor et al., 2013; Héja et al., 2022).

Based on our cross-section (Figure 5b), the R syncline is the trailing syncline of the HV thrust, which is interpreted to flatten into a shallow decollement at the base of Carnian marls. We suppose that, the VV anticline is a fault-bend fold, which developed above a second, deeper ramp of the HV thrust (Figure 5b). This deeper ramp of the HV thrust is possibly emerging from a deeper decollement, although the level of this decollement is unknown.



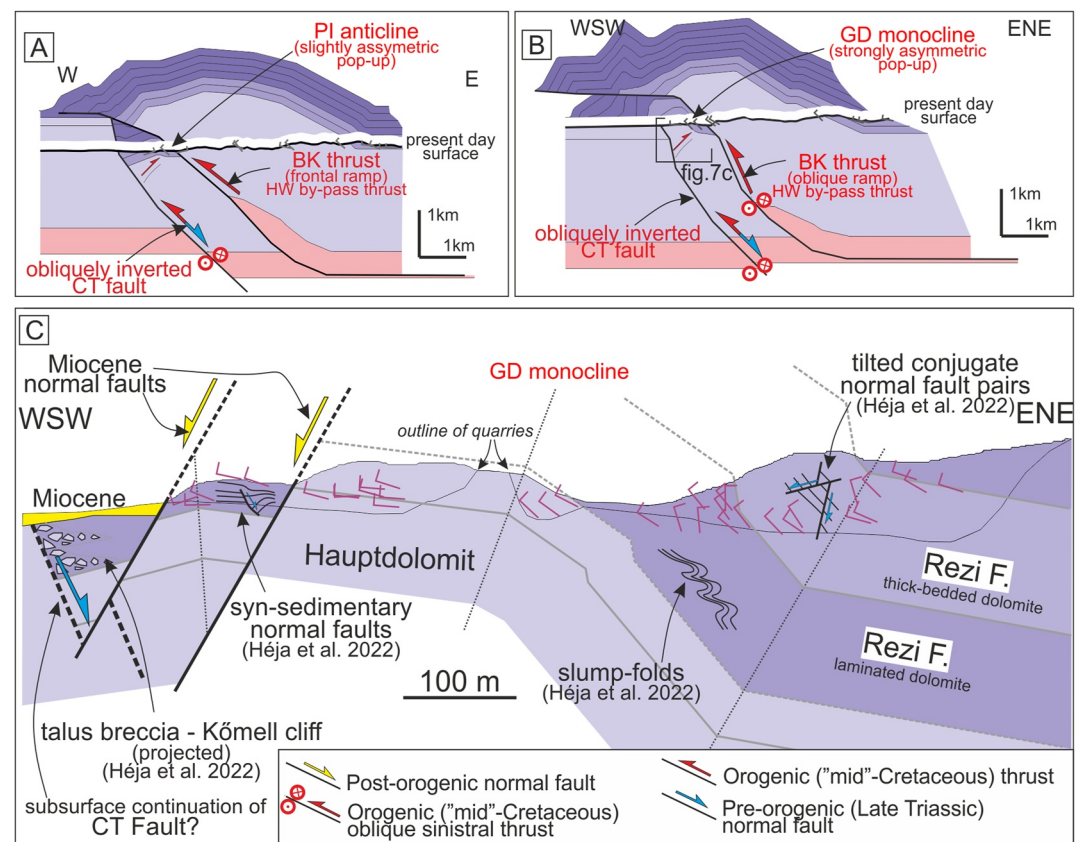


**Figure 7.** Cross-sections across the southern Keszthely Hills (for location see Figures 5a and 6a); (a) W–E striking section across the PI anticline and the BK anticline; (b) WSW–ENE striking section across the GD monocline and the BK anticline; (c) Cross-section across the GD monocline, showing the most important second-ordered structures related to the pre-orogenic extension (for detailed description see Héja et al., 2022).

According to Linzer and Tari (2012) the Paleozoic shales, the Lower Triassic marls, or the Middle Triassic basinal formations are possible levels for such a deep decollement (Figure 3). The BK anticline represents the hanging wall anticline of the west-directed BK thrust on the eastern limb of the VV anticline (Figure 5b). We propose that the BK thrust ramps up from the level of base Carnian marls, just like the shallow ramp of the HV thrust.

The SM fault and the VA syncline are dissected by several NW–SE trending sinistral strike-slip faults, which merge toward the west (Figure 5a). Based on the map-view pattern, these faults lose offset to the NW, and just slightly offset the R syncline. Therefore, these faults can be considered as syn-folding tear-faults, which accommodate differential shortening (Héja et al., 2018). The southern branch of these sinistral faults is continuing into the ED fault, therefore this fault was possibly active as a strike-slip (transfer) fault during the Cretaceous shortening (Figure 5a).

In contrast with the aforementioned N–S trending folds and thrust, the southern part of the KH is characterized by variously oriented compressional structures (Figure 6a). In our opinion this phenomenon is related to the oblique inversion of the strongly segmented CT fault. The N–S striking BK thrust and the associated anticline becomes gradually NW–SE trending southward where approaching the NW–SE-striking eastern segment of the Late Triassic CT fault (Figure 6a). Taking into consideration E–W transport direction during Cretaceous shortening, sinistral thrusting can be supposed on the NW–SE striking oblique ramp of the BK thrust. The western segment of this oblique ramp of the BK thrust runs across the hanging wall block of a pre-existing CT fault (Figure 7b), and therefore it can be considered as an oblique hanging wall by-pass thrust (Figure 5a). Based on the map-view pattern (Figure 5a) the BK thrust cut into the footwall of the CT fault further to the southeast (southeast from to GD monocline). Accordingly, this southernmost segment of the BK thrust represents an oblique footwall short-cut (Figure 5a), although the syn-rift Rezi Dolomite does not preserved in the hanging wall of the BK thrust.

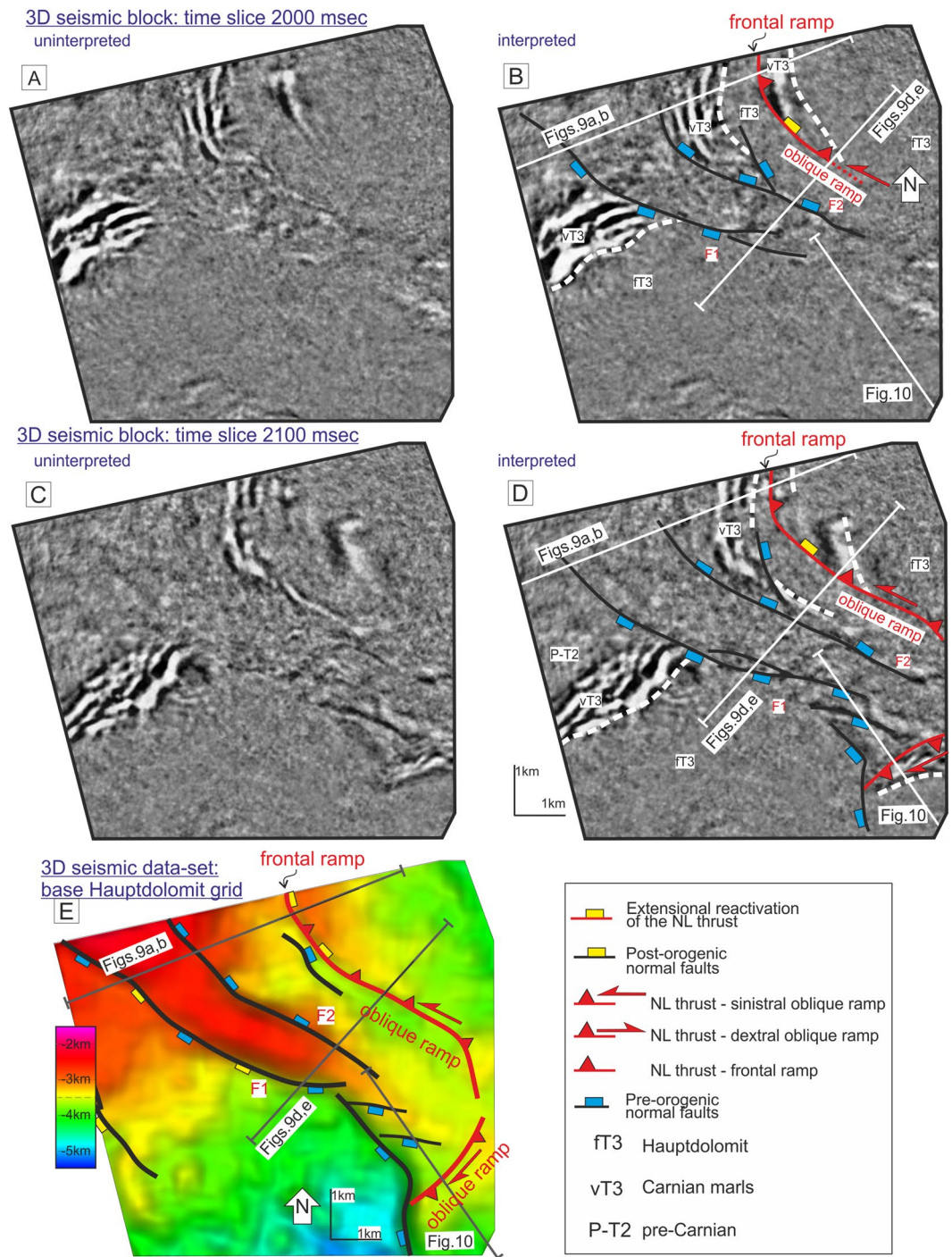


**Figure 8.** Pre-orogenic normal faults (F1 and F2) and the Cretaceous NL thrusts on time slices and depth map in the Zala Basin. (a and b) Uninterpreted and interpreted time-slice at 2,000 msec TWT depth (approximately 3.3 km below sea-level); (c and d) uninterpreted and interpreted time-slice at 2,100 msec TWT depth (approximately 3.5 km below sea-level); (e) Depth map of the base-Hauptdolomit in km below sea-level. For location of the 3D data set see Figure 2a.

Based on the cross-sections of Figures 7a and 7b the overthrust beds of the Hauptdolomit are laterally steepening south ward in the hanging wall of the BK thrust. This characteristic along-strike variations indicates the south ward steepening of the BK thrust approaching the CT fault (Figures 7a and 7b).



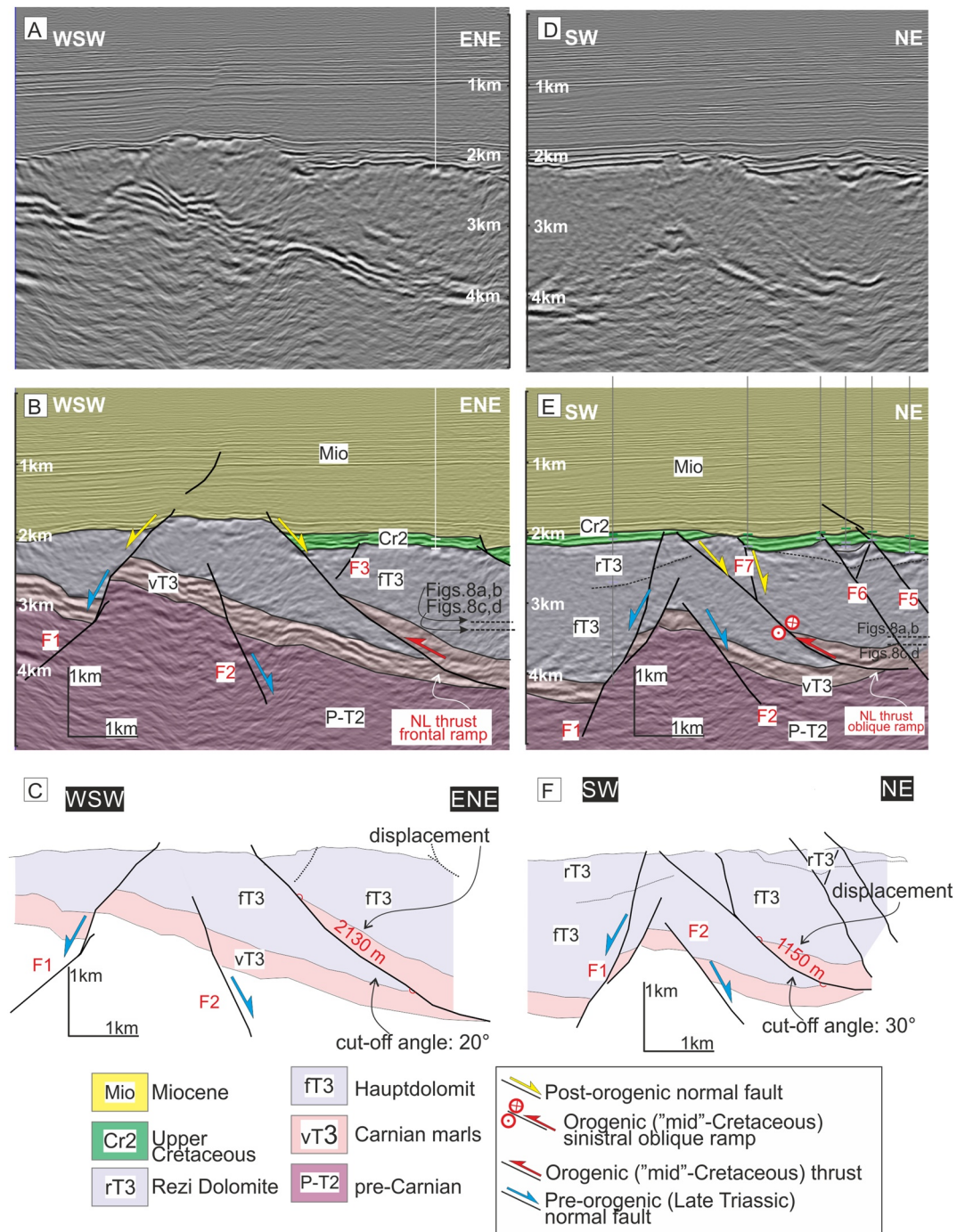


**Figure 9.** (a–c) Section across the N-S striking frontal ramp of the NL thrust; (d–f) Section across the NW-SE striking oblique ramp of the NL thrust; (a and d) uninterpreted, (b and e) interpreted; (c and f) restoration of the post-orogenic negative inversion; for location of the sections see Figure 8.

Two folds, with few hundreds meter of wavelength were identified by Héja et al. (2022), adjacent to the N- to NW-striking segments of the BK thrust (PI—Pilinkán anticline, GD—Gyenesdiás monocline). They are located both in the front of the BK thrust and in the immediate hanging wall of the CT fault (Figure 6a). The presence of Late Triassic sedimentary breccia, slumps, and tilted conjugate normal fault pairs indicates the proximity of the CT fault along the PI anticline and the GD monocline (Figures 6a and 7c; For detailed description see Héja et al., 2018, 2022). The N–S trending PI anticline (Figure 6d) is east directed and slightly asymmetric (Figure 7a).



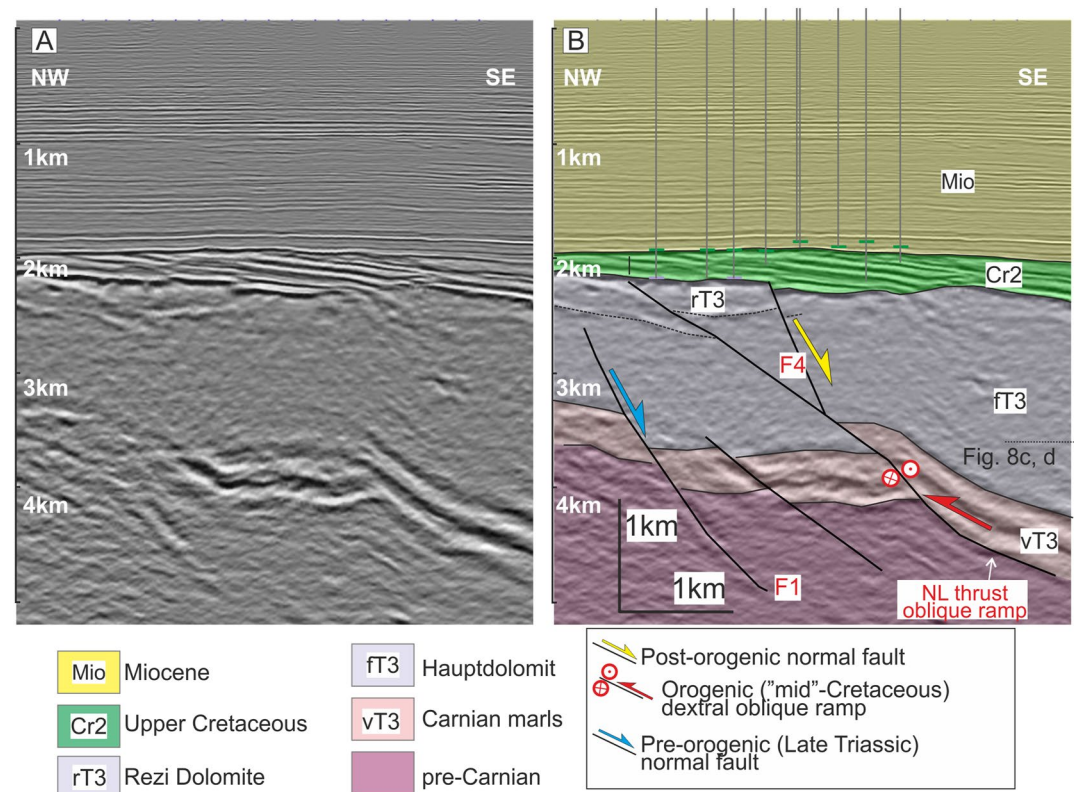


**Figure 10.** Section across the NE-SW striking oblique ramp of the NL thrust; (a) uninterpreted; (b) interpreted; for location of the section see Figure 8.

The southern displaced continuation of this fold is the GD monocline, which is situated closer to the CT fault (Figure 6a). Similarly to the PI anticline, the GD monocline is also east vergent, but it is NNW-SSE trending (Figure 6e) and more asymmetric (Figures 7b and 7c). In our opinion, the opposite vergency of these folds is related to blind back-thrusts coming from the eastern, reactivated segment of the CT fault (hanging wall breakthrough thrust following the term of Bonini et al., 2012), and the PI anticline and the GD monocline represent asymmetric pop-up structures (Figures 7a and 7b).

In the more distal foreland of the BK thrust laterally short, few hundred meter wavelength NE-SW trending folds occur, namely the PA (Pajtika) syncline (Figure 6b) and the MK (Molnárkő) anticline (Figure 6c). These oblique folds developed directly on the relay ramp, which connects the two main segments of the Late Triassic CT fault (Figure 6a). In our interpretation, the formation of these laterally short oblique folds was due to the inversion of minor faults that initially breached this relay ramp.

## 5.2. The Role of Pre-Existing Normal Faults in the Formation of the Curved NL (Nagylengyel) Thrust—Description of the 3D Seismic Data Set of the Zala Basin

### 5.2.1. Pre-Orogenic Normal Faults of the Zala Basin

Structures of the Mesozoic basement are outlined on 3D seismic reflection data: mostly based on the high amplitude reflections of the Carnian marls. This reflection package can be detected all along the southwestern TR, and it is drilled by the Keh-3 well between the KH and the present 3D data set (Figure 2b). One of the most significant structures of this seismic data set is a horst, which is enclosed by the F1 and F2 normal faults (Figures 8–10). These NW-SE striking normal faults (Figures 8b, 8d and 8e) have pronounced displacement on the high amplitude reflections of the Carnian marls on all sections (Figures 9b, 9e and 10b). Faint reflections appear within the thick non-reflective body of the Upper Triassic dolomites (Figures 9e and 10b), which can be considered as the base of Rezi Dolomite based on well data. The southern two seismic sections (Figures 9e and 10b) show that the

F1 and F2 faults are sealed by the base of the Rezi Dolomite, and the underlying Hauptdolomit is significantly thicker in the hanging wall than in the footwall of these faults. Based on that, the F1 and F2 normal faults can be interpreted as Late Triassic structures. The north-western part of the F1 fault suffered extensional reactivation later, since the fault generated significant offset in the base Upper Cretaceous and the base-Miocene horizons (Figure 9b). On the basis of F1 and F2 faults, the direction of Triassic extension was NE-SW, which is in accordance with the structural data of the KH (see Section 5.1.1).

### 5.2.2. Cretaceous Contractional Structures of the Zala Basin

The N-S trending major folds of the Zala Basin (NL and SD syncline on Figure 2a) suggest that the direction of Eoalpine shortening was E-W, similarly like in the KH. One of the most significant thrusts of the Zala Basin is the NL thrust, which is visible on the featured seismic 3D data set (Figures 8–10). The high amplitude Carnian marls are overthrust above the non-reflective Hauptdolomite along this west-directed thrust. Therefore the NL thrust is nicely outlined on the two featured horizontal time slices (Figures 8a–8d) and on the grid of the base Hauptdolomit horizon (Figure 8e). The frontal ramp of the thrust is N-S-striking at the northern edge of the 3D block, then southward it curves to a NW-SE striking oblique ramp, as it approaches the F2 normal fault (Figures 8b, 8d and 8e). South from the southeastern tip point of the F2 fault, the NL thrust turns back, and it has another, NE-SW striking oblique ramp along its southern part. Oblique, sinistral thrusting can be supposed on the NE dipping oblique ramp (Figures 8b, 8d and 8e), whereas dextral thrusting is presumed on the SE dipping oblique ramp (Figures 8d and 8e), if the tectonic transport was from East to west during Cretaceous shortening.

The presented sections (Figures 9 and 10) are perpendicular to the different segments of the NL thrust. The ENE-WSW striking section (Figures 9a and 9b) is running across the frontal ramp of the NL thrust, whereas the NE-SW striking (Figures 9d and 9e), and the NW-SE striking (Figure 10) cross-sections are crossing the NW-SE and the NE-SW striking oblique ramps of the NL thrust, respectively (Figure 8). Based on these cross-sections (Figures 9 and 10), the Carnian marls were thrust onto the Hauptdolomit along the footwall ramp of the NL (Nagylenyel) thrust. Toward the east, this ramp joins into a décollement at the level of base Carnian, similar to the HV and BK thrusts in the KH (Figures 5b, 7a and 7b). The trailing syncline of the NL thrust is visible on Figure 9e based on the reflection of the base Rezi Dolomite. This syncline is unconformably covered by Upper Cretaceous deposits. The NW-SE striking oblique ramp of the NL thrust climbs up through the hanging wall block of the pre-existing F2 normal fault (Figure 9e), and therefore it can be considered as an oblique hanging wall by-pass thrust, just like the BK thrust on Figure 7b. The location of this oblique ramp was likely controlled by F2 pre-existing normal fault, which is clearly visible on the horizontal time slices as well (Figure 8).

Taking into account the cut-off angle of the NL thrust and the Carnian marls, initially the NW-SE striking oblique ramp of the NL-thrust (Figure 9e) was steeper than the frontal ramp of the NL thrust (Figure 9c). We suppose similar along-strike variations in case of the BK thrust (Figures 7a and 7b).

Based on the separation of the base Upper Cretaceous horizon the N-S and NW-SE striking segments of the NL thrust were reactivated as a normal fault (Figures 8 and 9). In contrast, the southern NE-SW striking segment (Figure 10b) seems to be unaffected by negative inversion. Further synthetic and antithetic post-orogenic normal faults detach on the negatively inverted NL thrust (Figures 9b and 9e). The role of negative inversion in the development of the Pannonian Basin is demonstrated by a recent paper of Tari et al. (2021). According to Fodor et al. (2021) the direction of post-orogenic (mostly Miocene) extension was NE-SW in this area, which is roughly parallel with the direction of the northern and middle sections. Therefore we carried out section restorations in order to remove the effect of this post-orogenic negative inversion on the aforementioned sections (Figures 9c and 9f). Based on these restored sections, the NL thrust shows more than 2 km displacement along the frontal ramp (Figure 9c), whereas the apparent displacement (perpendicular to the thrust) is ~1.15 km along the NW-SE striking oblique ramp of the NL thrust (Figure 9f).

Most of the post-orogenic normal faults die out upward just above the base-Miocene horizon (F5 and F6 on Figure 9e), thus they represent the syn-rift faults of the Pannonian Basin. Some normal faults that offset the base Upper Cretaceous, but are sealed by the base-Miocene horizon demonstrate pre-Middle Miocene, but post-orogenic normal faulting (e.g., F3 on Figure 9b).

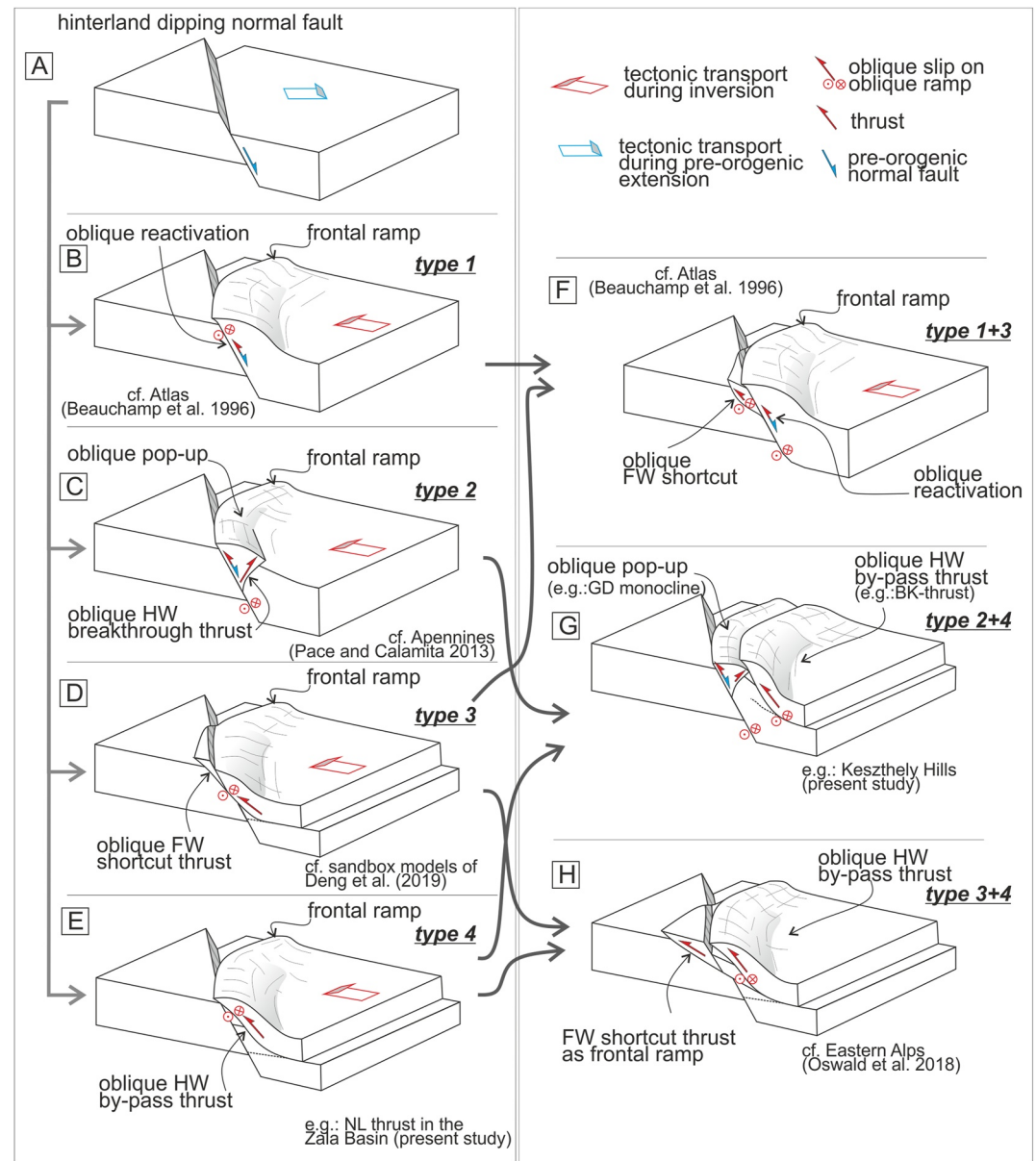


**Figure 11.** Modes of oblique inversion; (a) hinterland dipping normal fault prior to inversion; (b–e) Basic end-member models of oblique inversion based on Figure 4; (b) oblique reactivation of pre-orogenic normal fault; (c) oblique pop-up between a reactivated normal fault and a hanging wall breakthrough thrust; (d) oblique footwall shortcut thrust; (e) oblique hanging wall by-pass thrust; (f–h) variations and combinations of basic end-member models of oblique inversion; (f) combination of oblique reactivation and oblique footwall short-cut thrust; (g) combination of oblique pop-up and an oblique hanging wall by-pass thrust; (h) combination of an oblique hanging wall by-pass thrust and footwall short cut thrust.

## 6. Discussion

### 6.1. Classification of Inversion Related Oblique Ramps—Comparison With Natural and Analogue Model Examples

Oblique and lateral ramps are often inherited and related to pre-existing, rift-related normal faults in fold and thrust belts. Nonetheless, the geometric relationships between these structures are rarely described in detail. In this chapter we summarize the modes of oblique inversion (Figure 11) based on natural examples of the study area, and other orogens. We apply the section-view end-member models of inversional structures—introduced in Section 3 (Figure 4)—for the characterization and classification of oblique ramps. Based on that, we determine



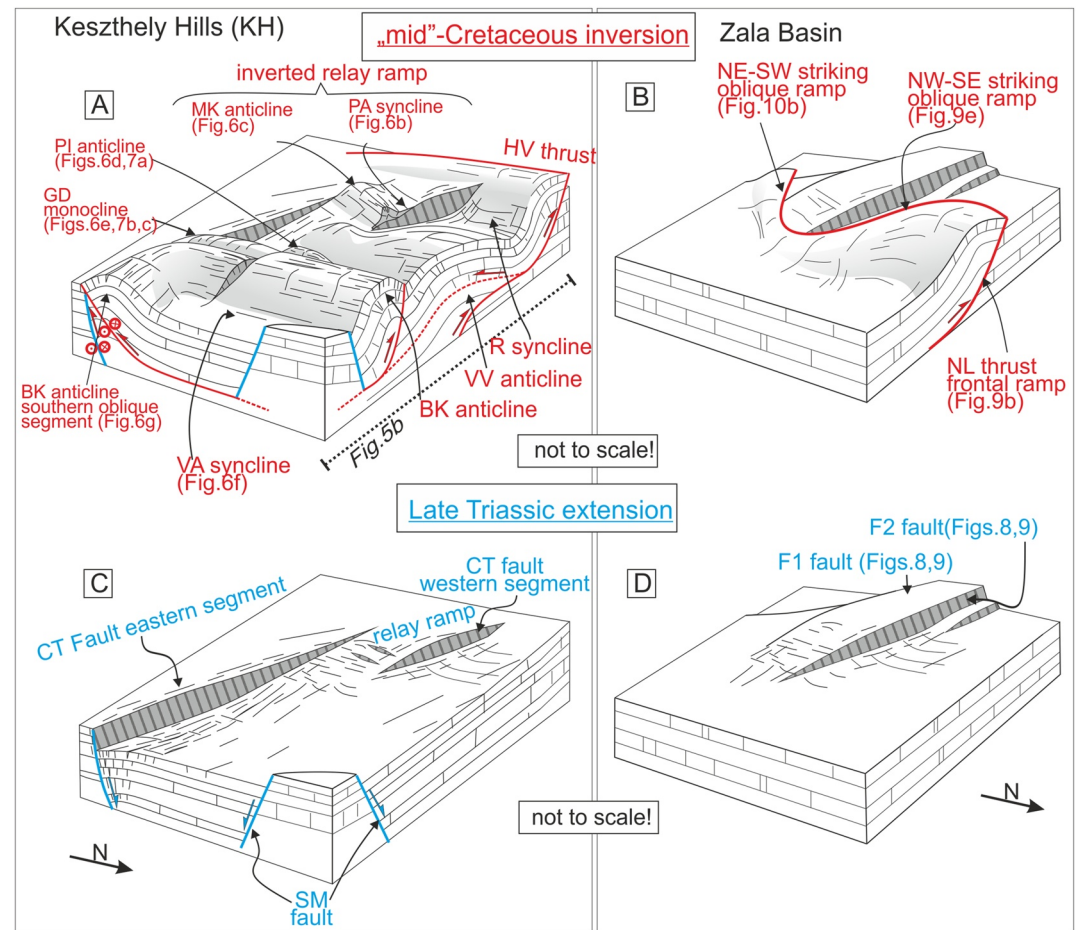


**Figure 12.** Schematic model of oblique inversion (a and c) in the Keszthely Hills (b and d) and in the Zala Basin. (c and d) Show the configuration of the Late Triassic normal faults and grabens, whereas (a and b) illustrate the geometry of inversion.

four end-member models for oblique inversion, these are: oblique reactivation (type 1 on Figure 11b); oblique hanging wall breakthrough thrust (type 2 on Figure 11c); oblique footwall shortcut thrust (type 3 on Figure 11d); oblique hanging wall by-pass thrust (type 4 on Figure 11e).

In the case of oblique reactivation the inversion related oblique ramp uses the surface of inherited normal fault (type 1 on Figure 11b). We consider the eastern segment of the CT fault as such type of oblique ramp. Similar examples for oblique reactivation of pre-existing normal faults are known for example, from the Atlas Mountains (Beauchamp et al., 1996; Saïd et al., 2011). Our results show that not only the graben bounding normal faults, but the breaching faults on relay ramps may also suffer inverse reactivation. We speculate that the PA syncline and the MK anticline developed by the oblique reactivation (Figure 12a) of breaching faults on the relay ramp of the CT fault (Figure 12c). Similar oblique inversion of pre-existing breaching faults has been described from the Iberian Chain by De Vicente et al. (2009). One of the most characteristic feature of these inverted relay ramps is that, they represent laterally short fold segments, similarly to the MK anticline and PA syncline.

Oblique hanging wall breakthrough thrusts represent another type of oblique ramps (type 2 on Figure 11c). Oblique pop-up structures may form between reactivated normal faults and hanging wall breakthrough thrusts. We classify the GD monocline as such type of oblique pop-up structure (Figure 12a). Similar oblique ramps (push-up structures) have been reported by Pace and Calamita (2013) from the Apennines. In these examples of Pace and Calamita (2013) the oblique pop-up structures are bounded by several branches of fore and back-thrusts, producing flower-like geometry.

Footwall short-cut thrusts frequently follow the direction of pre-orogenic normal faults, which strikes oblique to the direction of shortening. These oblique footwall short-cut thrusts form another type of oblique ramps (type 3

on Figure 11d). We consider the southeastern segment of the BK thrust as such type of oblique ramp (Figure 5a). Oblique footwall short cut thrusts have been reported by the sand box models of Deng et al. (2019) and by the natural examples from the Atlas Mountains (Beauchamp et al., 1996).

Oblique hanging wall by-pass thrusts (type 4 on Figure 11e) represent the fourth end-member model of oblique inversion. In our study, the NW-SE striking oblique ramp of the NL thrust (Figure 12b) and the oblique ramp of the BK thrust (Figure 12a), east of the GD monocline provide nice examples for oblique hanging wall by-pass thrusts. The oblique ramp of the Variscan frontal thrust in the Ardennes represents a large-scale example for an oblique hanging wall by-pass thrust. The oblique ramp of this far-traveled allochthonous unit is localized by a set of hinterland dipping normal fault (Laurent et al., 2021).

Our and other natural examples show that these endmembers are often superposed on each other and lateral variation in the type of inversion may also occurs along the same oblique ramp. The BK thrust is a good example for the lateral variation in the style of oblique inversion: the frontal ramp of the BK thrust gradually turns into an oblique hanging wall by-pass thrust, that continues as an oblique footwall short-cut thrust southeast ward (Figure 5a). For superposition of different end-members the southeastern part of the KH is a good example. It represents such a complex zone of oblique ramps, where an oblique pop-up (GD monocline) in the hanging wall of the obliquely reactivated CT fault is superimposed onto the oblique hanging wall by-pass ramp of the BK thrust (Figure 11g). Similar complex zones of oblique ramps are known from other orogenies. Combination of an oblique footwall short-cut thrust and reactivated normal faults (Figure 11f) has been described by Beauchamp et al. (1996) from the Atlas Mountains. Interaction between low angle thrusts and reactivated normal faults create a regional scale oblique ramp in the NW Taiwan fold and thrust belt (Lacombe et al., 2003)

Sand-box models of Yagupsky et al. (2008) serve excellent analogies for our interpretations (Figure 13b). Yagupsky et al. (2008) investigated the role of a pre-existing oblique graben on the temporal evolution of the subsequent fold and thrust belt. The extensional graben in one of their models strikes at  $45^\circ$  to the shortening. These authors found that an oblique pop-up structure developed by the reactivation of the graben bounding normal faults at the early stage of inversion, and the inversion of the graben was migrating toward the foreland (Figure 13b). The PI anticline and the more pronounced GD monocline can be interpreted as a similar pop-up structure in the hanging wall of the reactivated eastern segment of the CT fault (Figure 13a). The CT fault suffered less inversion west of the PI anticline than in the area of GD monocline, which can be explained by the west-directed, forelandward migration of inversion. Due to increasing contraction, the oblique pop-up was cut by a young thrust perpendicular to the shortening in the model of Yagupsky et al. (2008) (Figure 13b). The newly formed thrust branches from the previously inverted normal fault, and it corresponds to the N-S striking BK thrust, which continues in a NW-SE striking oblique ramp in the vicinity of the pre-existing CT fault (Figure 13a).

## 6.2. Reactivation or Locking? The Importance of Orientation of the Fault

It is an important question, whether a pre-existing normal fault suffered reactivation, or they remained locked during contractional deformation. The mode of fault reactivation depends on a number of parameters including fluid pressure (Sibson, 2009), weakness of the fault zone (Ruh, 2019), the type of the stress-field, and the orientation and the dip of the fault (Sassi et al., 1993).

Our data set allows to investigate the effect of the orientation of the normal fault on fault reactivation (Figure 13c). Based on our examples, we found that faults that strike at low angle to the shortening remained locked during inversion (NV fault, CT fault western segment, F1 and F2 faults). Faults, that strike at higher angle to shortening reactivated as an oblique inverse (CT fault eastern segment) or sinistral strike-slip (ED fault) fault during inversion (Figure 13c). The only exception was the Szent Miklós fault, which strikes almost perpendicular to the direction of shortening, but remained locked during inversion. Our results are in accordance with the sandbox models of Deng et al. (2019), who found that reactivation of pre-existing normal faults is obvious if the normal faults strike at high angle to the shortening direction ( $40^\circ$ – $90^\circ$ ). In contrast, Brun and Nalpas (1996) obtained strongly different results from similar sandbox models. According to these authors reactivation of normal faults occurs, if the angle between the strike of the normal faults and the direction of shortening is less than  $45^\circ$ .

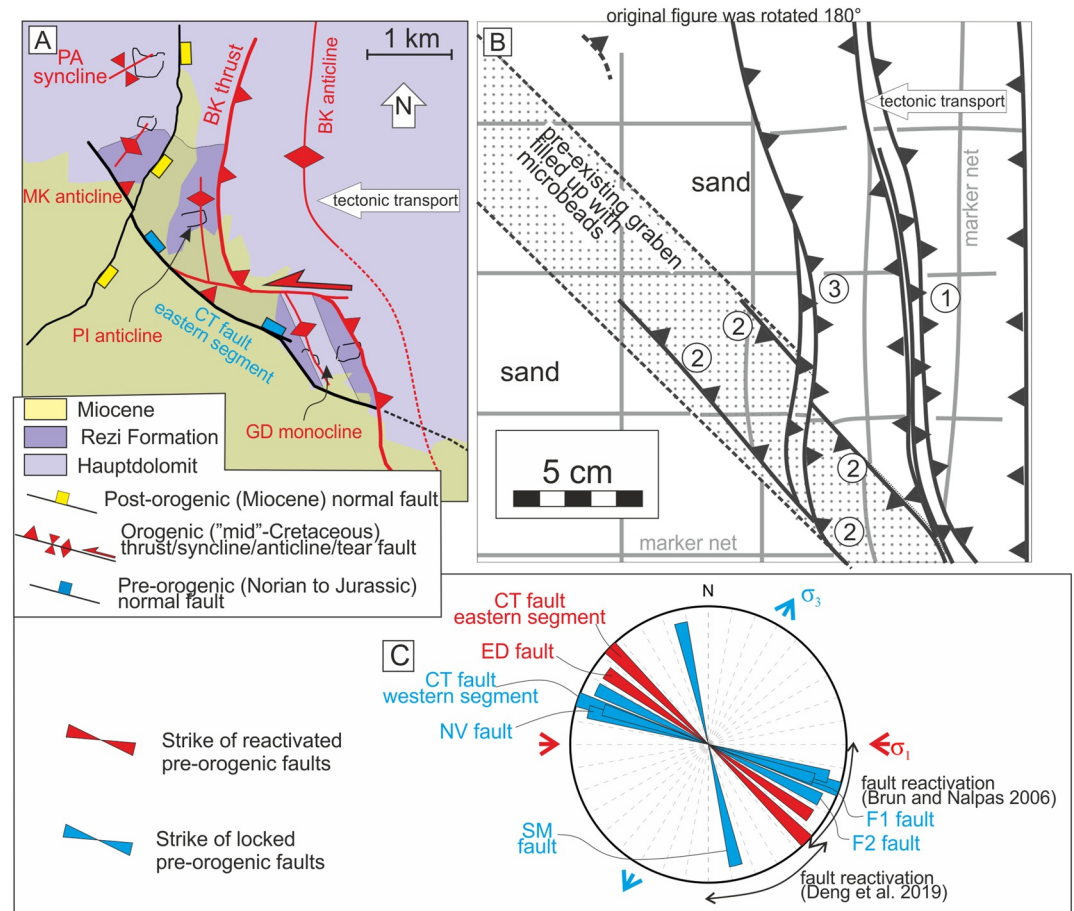


**Figure 13.** Comparison of (a) the structure of the southern Keszthely Hills, and (b) the analogue model of Yagupsky et al. (2008). Panel (b) was redrawn based on the original photo. For location of the map see Figure 6a. (c) Rose diagram, showing the role of normal fault orientation on inverse reactivation.

### 6.3. Oblique Inversion in the Eoalpine Orogeny: Local and Regional Implication

The European Alps are the result of two orogenic event (Figure 1), where the Cretaceous (Eoalpine) formation of the Austroalpine nappe-system was overprinted by the Cenozoic collision of these Adria derived units and the European margin (Schmid et al., 2004). Inversion of former rifted margins is a widely known phenomenon in the Cenozoic evolution of the Alpine orogeny (e.g., Boutoux et al., 2014; Butler et al., 2006; Granado et al., 2017; Tari et al., 2020; Ustaszewski & Schmid, 2006). However, the role of structural inheritance during the Cretaceous formation of the Austroalpine nappes (Eoalpine orogeny) is much less studied. This is especially true for the Transdanubian Range, which is the uppermost unit of the Austroalpine nappe system. The variation seen in the orientations of Cretaceous compressional structures in the TR have been traditionally explained by polyphase folding, where different fold populations represent individual phases of compression (for a detailed review of previous works see Héja et al., 2022). In contrast, our work shows that variously oriented folds and thrusts developed due to the oblique inversion during one single shortening phase (Figure 12). This type of structural inheritance has been only sporadically documented in the Austroalpine region: complex structural geometry of the Achensee area shows many similarities to the examples of the present study. In this western part of the Northern Calcareous Alps the E-W trending Karwendel and Thiersee synclines are linked by the N-S trending Unutz fold (Figure 6 of Ortner, 2003). The dilemma of poly-phase folding versus structural inheritance arises in this case, too. On one hand, the abrupt change in fold trend was explained by two-phases of shortening (e.g., Ortner, 2003), on the other hand, the Unutz fold developed above a transverse zone or oblique ramp, which was localized by a pre-existing Triassic-Jurassic normal fault (e.g., Behrmann & Tanner, 2006; Eisbacher & Brandner, 1996; Ortner & Gruber, 2012). Recently, Oswald et al. (2018) described how the Eoalpine Lechtal thrust recessed around a



pre-existing graben shoulder, which was later cut and emplaced by footwall short-cut thrusts in the Northern Calcareous Alps (Figure 11b). The first step of this inversion geometry is very similar to our finding in the Zala Basin, where the NL thrust makes a considerable recess around a pre-existing extensional horst (Figure 12b).

## 7. Conclusions

In this study, we present seismic and field observations that demonstrate the Cretaceous oblique inversion of a segmented Triassic graben system. The prevalent orientation of Cretaceous folds and thrusts are N-S trending in the study area, but two additional directions of fold and thrusts also occur locally. One of these are NW-SE striking oblique ramps, which were localized by pre-existing normal faults. The others are NE-SW trending folds with a limited strike-parallel length that can be associated to inverted breaching faults, which connected the laterally segmented pre-existing normal faults. Our examples show that these three populations of folds and thrusts developed during one single shortening phase due to E-W regional contraction, rather than that of multiphase folding, which has been the general structural interpretation in the TR to date. Inversion oblique ramps of the study area are represented by reactivated normal faults, oblique hanging wall breakthrough thrusts, oblique footwall short cut thrusts, and oblique hanging wall by-pass thrusts. During shortening, only those pre-orogenic normal faults were reactivated, that enclosed a high angle to the direction of shortening.

Our study is one of the first documentations of oblique inversion in the Austroalpine (Eoalpine) orogeny. Similar type of structural inheritance can be expected in other parts of the Austroalpine nappes, which need further research.

## Data Availability Statement

The seismic data set was made available by MOL Hungarian Oil and Gas Plc. Quarry managers permitted access to the visited quarries (Dolomit Ltd., Molnárkő Ltd., and Pajtika Ltd.). The data product introduced in this work is available on an online open access repository (Héja, 2020). Stereoplots were plotted by the software InnStereo (Schönberg, 2015).

## Acknowledgments

This work was supported by the Hungarian Scientific Research Fund NKFIH OTKA 113013. The manuscript has been finished with the support of the grant NKFIH OTKA 134873. The first version of this manuscript was written during the CEEPUS stay of the first author in Innsbruck. The first author was also supported by the scholarships UNKP. English language and style of the manuscript was improved by D. Novak. The authors acknowledge the academic license of Midland Valley Move software, which were used for section creation and reconstruction. Very detailed and constructive reviews of Oscar Fernandez, and the useful remarks and comments of Pablo Granada, Dušan Plašienka, Gábor Tari, and the editor (Ernst Willingshofer) significantly improved the manuscript.

## References

- Amilibia, A., McClay, K. R., Sàbat, F., Muñoz, J. A., & Roca, E. (2005). Analogue modelling of inverted oblique rift systems. *Geologica Acta: An international earth science journal*, 3(3), 251–271. Retrieved From <https://raco.cat/index.php/GeologicaActa/article/view/82307>
- Amilibia, A., Sàbat, F., McClay, K. R., Muñoz, J. A., Roca, E., & Chong, G. (2008). The role of inherited tectono-sedimentary architecture in the development of the central Andean mountain belt: Insights from the Cordillera de Domeyko. *Journal of Structural Geology*, 30, 1520–1539. <https://doi.org/10.1016/j.jsg.2008.08.005>
- Apotria, T. G., Snedden, W. T., Spang, J. H., & Wilitshko, D. V. (1992). Kinematic models of deformation at an oblique ramp. In McClay, K. R. (Ed.), *Thrust tectonics* (pp. 141–154). [https://doi.org/10.1007/978-94-011-3066-0\\_12](https://doi.org/10.1007/978-94-011-3066-0_12)
- Beauchamp, W., Barazangi, M., Demnati, A., & El Alji, M. (1996). Intracontinental rifting and inversion: Missouri basin and Atlas Mountains, Morocco. *AAPG Bulletin*, 80, 1459–1482. <https://doi.org/10.1306/64ed9a60-1724-11d7-8645000102c1865d>
- Behrmann, J. H., & Tanner, D. C. (2006). Structural synthesis of the northern Calcareous Alps, TRANSALP segment. *Tectonophysics*, 414, 225–240. <https://doi.org/10.1016/j.tecto.2005.10.018>
- Bonini, M., Sani, F., & Antonielli, B. (2012). Basin inversion and contractional reactivation of inherited normal faults: A review based on previous and new experimental models. *Tectonophysics*, 522–523, 55–88. <https://doi.org/10.1016/j.tecto.2011.11.014>
- Boutoux, A., Bellahsen, N., Lacombe, O., Verlaquet, A., & Mouthereau, F. (2014). Inversion of pre-orogenic extensional basins in the external Western Alps: Structure, microstructures and restoration. *Journal of Structural Geology*, 60, 13–29. <https://doi.org/10.1016/j.jsg.2013.12.014>
- Brun, J. P., & Nalpas, T. (1996). Graben inversion in nature and experiments. *Tectonics*, 15, 677–687. <https://doi.org/10.1029/95tc03853>
- Budai, T., Császár, G., Csillag, G., Dudko, A., Koloszá, L., & Majoros, G. (1999). *Geology of the Balaton Highland, explanation to the geological map of the Balaton Highland (1:50 000)* (p. 257). Geological Institute of Hungary.
- Budai, T., Csillag, G., Dudko, A., & Koloszá, L. (1999). *Geological map of the Balaton Highland (1:50 000)*. Geological Institute of Hungary.
- Budai, T., & Koloszá, L. (1987). Stratigraphic investigation of the Norian-Rhaetian formations in the Keszthely Mountains (in Hungarian with English abstract). *Földtani Kozlony*, 117, 121–130.
- Budai, T., & Vörös, A. (2006). Middle Triassic platform and basin evolution of the southern Bakony Mountains (Transdanubian range, Hungary). *Rivista Italiana di Paleontologia e Stratigrafia*, 112(3), 359–371.
- Butler, R. W., Tavarnelli, E., & Grasso, M. (2006). Structural inheritance in mountain belts: An Alpine–Apennine perspective. *Journal of Structural Geology*, 28, 1893–1908. <https://doi.org/10.1016/j.jsg.2006.09.006>
- Csillag, G., Budai, T., Gyalog, L., & Koloszá, L. (1995). Contribution to the upper Triassic geology of the Keszthely Mountains (Transdanubian range), western Hungary. *Acta Geologica Hungarica*, 38(2), 111–129.
- Csontos, L., & Nagymarosy, A. (1998). The mid-Hungarian line: A zone of repeated tectonic inversion. *Tectonophysics*, 297, 51–71. [https://doi.org/10.1016/s0040-1951\(98\)00163-2](https://doi.org/10.1016/s0040-1951(98)00163-2)
- Deng, H., Koyi, H. A., & Zhang, J. (2019). Modelling oblique inversion of pre-existing grabens. *Geological Society, London, Special Publications*, 487, 263–290. <https://doi.org/10.1144/sp487.5>

- De Vicente, G., Vegas, R., Muñoz-Martín, A., Van Wees, J. D., Casas-Sáinz, A., Sopeña, A., & Fernández-Lozano, J. (2009). Oblique strain partitioning and transpression on an inverted rift: The Castilian Branch of the Iberian Chain. *Tectonophysics*, 470(3–4), 224–242. <https://doi.org/10.1016/j.tecto.2008.11.003>
- Dogliani, C. (1987). Tectonics of the dolomites (southern Alps, northern Italy). *Journal of Structural Geology*, 9, 181–193. [https://doi.org/10.1016/0191-8141\(87\)90024-1](https://doi.org/10.1016/0191-8141(87)90024-1)
- Dohr, G. (1981). Geophysikalische untersuchungen im gebiet der tiefbohrung Vorderriß 1. *Geologica Bavarica*, 81, 55–64.
- Eisbacher, G., & Brandner, R. (1996). Superposed fold-thrust structures and high-angle faults, Northwestern Calcareous Alps, Austria. *Eclogae Geologicae Helveticae*, 89(1), 553–571.
- Fodor, L., Balázs, A., Csillag, G., Dunkl, I., Héja, G., Jelen, B., et al. (2021). Crustal exhumation and depocenter migration from the Alpine orogenic margin towards the Pannonian extensional back-arc basin controlled by inheritance. *Global and Planetary Change*, 201, 103475. <https://doi.org/10.1016/j.gloplacha.2021.103475>
- Fodor, L., Uhrin, A., Palotás, K., Selmecezi, I., Makk, T. Á., Rižnar, I., et al. (2013). *Geological and structural model of the Mura–Zala Basin and its rims as a basis for hydrogeological analysis (in Hungarian with English abstract)* (pp. 47–92). Annual Report of the Geological Institute of Hungary.
- Granado, P., Ferrer, O., Muñoz, J. A., Thöny, W., & Strauss, P. (2017). Basin inversion in tectonic wedges: Insights from analogue modelling and the Alpine–Carpathian fold-and-thrust belt. *Tectonophysics*, 703–704, 50–68. <https://doi.org/10.1016/j.tecto.2017.02.022>
- Gulyás, Á. (1991). *Jelentés a Keszthelyi-hegység és a Bakonyban 1990-ben a Plató program keretében végzett felszíni geofizikai mérésekről*. Budapest: Plató project 1990.
- Haas, J., Budai, T., & Raucsik, B. (2012). Climatic controls on sedimentary environments in the Triassic of the Transdanubian range (Western Hungary). *Palaeogeography, Palaeoclimatology, Palaeoecology*, 353–355, 31–44. <https://doi.org/10.1016/j.palaeo.2012.06.031>
- Haas, J., Jocháné-Edelényi, E., Gidai, L., Kaiser, M., Kretzoi, M., & Oravecz, J. (1984). Geology of the Sümeg area. *Geologica Hungarica - Serie Geologica*, 20, 353.
- Haas, J., Kovács, S., Krystyn, L., & Lein, R. (1995). Significance of Late Permian-Triassic facies zones in terrane reconstructions in the Alpine-North Pannonian domain. *Tectonophysics*, 242(1–2), 19–40. [https://doi.org/10.1016/0040-1951\(94\)00157-5](https://doi.org/10.1016/0040-1951(94)00157-5)
- Handy, M. R., Schmid, S. M., Bousquet, R., Kissling, E., & Bernoulli, D. (2010). Reconciling plate-tectonic reconstructions of Alpine Tethys with the geological–geophysical record of spreading and subduction in the Alps. *Earth-Science Reviews*, 102(3–4), 121–158. <https://doi.org/10.1016/j.earscirev.2010.06.002>
- Héja, G. (2020). *Collection: Cretaceous oblique inversion of a Late Triassic normal fault system in the western Transdanubian Range (TR)*. <https://doi.org/10.6084/m9.figshare.c.4607147.v1>
- Héja, G., Fodor, L., Csillag, G., Ortner, H., & Kövér, S. (2022). Complex deformation history of the Keszthely Hills, Transdanubian range, Hungary. *Central European Geology*, 65.
- Héja, G., Kövér, S., Csillag, G., Németh, A., & Fodor, L. (2018). Evidences for pre-orogenic passive-margin extension in a Cretaceous fold-and-thrust belt on the basis of combined seismic and field data (western Transdanubian Range, Hungary). *International Journal of Earth Sciences*, 107, 2955–2973. <https://doi.org/10.1007/s00531-018-1637-3>
- Horváth, F., Musitz, B., Balázs, A., Végh, A., Uhrin, A., Nádor, A., et al. (2015). Evolution of the Pannonian basin and its geothermal resources. *Geothermics*, 53, 328–352. <https://doi.org/10.1016/j.geothermics.2014.07.009>
- Kőrössi, L. (1988). Hydrocarbon geology of the Zala Basin in Hungary (in Hungarian). *Atalános Foldtani Szemle*, 23, 3–162.
- Lacombe, O., Mouthereau, F., Angelier, J., Chu, H. T., & Lee, J. C. (2003). Frontal belt curvature and oblique ramp development at an obliquely collided irregular margin: Geometry and kinematics of the NW Taiwan fold-thrust belt. *Tectonics*, 22(3), 9. <https://doi.org/10.1029/2002TC001436>
- Laurent, A., Averbuch, O., Beccaletto, L., Graveleau, F., Lacquement, F., Capar, L., & Marc, S. (2021). 3-D structure of the Variscan thrust front in northern France: New insights from seismic reflection profiles. *Tectonics*, 40, e2020TC006642. <https://doi.org/10.1029/2020TC006642>
- Linzer, H. G., & Tari, G. (2012). *Structural Correlation between the Northern Calcareous Alps (Austria) and the Transdanubian Central Range (Hungary)* (Vol. 100, pp. 249–266). American Association of Petroleum Geologists Memoir.
- Marques, F. O., & Nogueira, C. R. (2008). Normal fault inversion by orthogonal compression: Sandbox experiments with weak faults. *Journal of Structural Geology*, 30, 761–766. <https://doi.org/10.1016/j.jsg.2008.02.015>
- Marshak, S., Wilkerson, M., & Hsui, A. (1992). Generation of curved fold-thrust belts: Insight from simple physical and analytical models. In McClay, K. R. (Ed.), *Thrust tectonics* (pp. 83–92). [https://doi.org/10.1007/978-94-011-3066-0\\_7](https://doi.org/10.1007/978-94-011-3066-0_7)
- McClay, K. R. (1995). The geometries and kinematics of inverted fault systems; a review of analogue model studies. In Buchanan, J. G., & Buchanan, P. G. (Eds.), *Basin inversion*, 88 (Vol. 88, pp. 97–118). Geological Society of London Special Publication. <https://doi.org/10.1144/gsl.sp.1995.088.01.07>
- Muñoz, J.-A., Beamud, E., Fernández, O., Arbués, P., Dinarés-Turell, J., & Poblet, J. (2013). The Ainsa Fold and thrust oblique zone of the central Pyrenees: Kinematics of a curved contractional system from paleomagnetic and structural data. *Tectonics*, 32, 1142–1175. <https://doi.org/10.1002/tect.20070>
- Ortner, H. (2003). Cretaceous thrusting in the western part of the Northern Calcareous Alps (Austria)—Evidences from synorogenic sedimentation and structural data. *Mitteilungen der Österreichischen Geologischen Gesellschaft*, 94, 63–77.
- Ortner, H., & Gruber, A. (2012). 3D-model of complex km-scale fold structures using laserscanning images: The Achensee region, western Northern Calcareous Alps, Austria. *Geophysical Research Abstracts*, 14. Retrieved From <https://ui.adsabs.harvard.edu/abs/2012EGUGA.14.3102O>
- Oswald, P., Ortner, H., & Gruber, A. (2018). Deformation around a detached half-graben shoulder during nappe stacking (Northern Calcareous Alps, Austria). *Swiss Journal of Geosciences*, 112(1), 23–37. <https://doi.org/10.1007/s00015-018-0333-4>
- Pace, P., & Calamita, F. (2013). Push-up inversion structures vs. fault-bend reactivation anticlines along oblique thrust ramps: Examples from the Apennines fold-and-thrust belt (Italy). *Journal of the Geological Society*, 171, 227–238. <https://doi.org/10.1144/jgs2013-053>
- Pedraza, A., Ruiz-Constán, A., García-Senz, J., Azor, A., Marín-Lechado, C., Ayala, C., et al. (2020). Evolution of the South-Iberian paleomargin: From hyperextension to continental subduction. *Journal of Structural Geology*, 138, 104122. <https://doi.org/10.1016/j.jsg.2020.104122>
- Pocsai, T., & Csontos, L. (2006). Late Aptian–early Albian syn-tectonic facies pattern of the Tata limestone formation (Transdanubian range, Hungary). *Geologica Carpathica*, 57, 15–27.
- Ramsay, J. G. (1967). *Folding and Fracturing of Rocks* (p. 568). McGraw-Hill.
- Ratschbacher, L., Frisch, W., Linzer, G., & Merle, O. (1991). Lateral extrusion in the eastern Alps. Part 2: Structural analysis. *Tectonics*, 10, 257–271. <https://doi.org/10.1029/90TC02623>
- Royden, L. H. (1993). The tectonic expression of slab pull at continental convergent boundaries. *Tectonics*, 12, 303–325. <https://doi.org/10.1029/92tc02248>

- Ruh, J. B. (2019). Effects of fault-weakening processes on oblique intracontinental rifting and subsequent tectonic inversion. *American Journal of Science*, 319, 315–338. <https://doi.org/10.2475/04.2019.03>
- Said, A., Baby, P., Chardon, D., & Ouali, J. (2011). Structure, paleogeographic inheritance, and deformation history of the southern Atlas foreland fold and thrust belt of Tunisia. *Tectonics*, 30, TC6004. <https://doi.org/10.1029/2011TC002862>
- Sassi, W., Colletta, B., Balé, P., & Paquereau, T. (1993). Modelling of structural complexity in sedimentary basins: The role of pre-existing faults in thrust tectonics. *Tectonophysics*, 226, 97–112. [https://doi.org/10.1016/0040-1951\(93\)90113-x](https://doi.org/10.1016/0040-1951(93)90113-x)
- Sasvári, Á. (2008). Shortening-related deformation in the Gerecse Mts, Transdanubian range, Hungary. *Földtani Közlemények*, 138(4), 385–402.
- Sasvári, Á. (2009). *Középső-kréta rövidülési deformáció és szerkezeti betemetődés a Gerecse területén* (p. 164). Department of Applied and General Geology, Eötvös University.
- Schmid, S. M., Bernoulli, D., Fügenschuh, B., Matenco, L., Schefer, S., Schuster, R., et al. (2008). The Alpine-Carpathian-Dinaridic orogenic system: Correlation and evolution of tectonic units. *Swiss Journal of Geosciences*, 101, 139–183. <https://doi.org/10.1007/s00015-008-1247-3>
- Schmid, S. M., Fügenschuh, B., Kissling, E., & Schuster, R. (2004). Tectonic map and overall architecture of the Alpine orogen. *Eclogae Geologicae Helveticae*, 97(1), 93–117. <https://doi.org/10.1007/s00015-004-1113-x>
- Schmid, S. M., Fügenschuh, B., Kounov, A., Mañenco, L., Nievergelt, P., Oberhänsli, R., et al. (2020). Tectonic units of the Alpine collision zone between Eastern Alps and western Turkey. *Gondwana Research*, 78, 308–374. <https://doi.org/10.1016/j.gr.2019.07.005>
- Schönberg, T. (2015). Retrieved From <https://finnstereo.github.io/>
- Sibson, R. H. (2009). Rupturing in overpressured crust during compressional inversion—The case from NE Honshu, Japan. *Tectonophysics*, 473, 404–416. <https://doi.org/10.1016/j.tecto.2009.03.016>
- Tari, G. (1994). *Alpine Tectonics of the Pannonian Basin PhD Dissertation* (p. 501). Houston: Rice University.
- Tari, G., Arbouille, D., Schléder, Z., & Tóth, T. (2020). Inversion tectonics: A brief petroleum industry perspective. *Solid Earth*, 11, 1865–1889. <https://doi.org/10.5194/se-11-1865-2020>
- Tari, G., Bada, G., Beidinger, A., Csizmeg, J., Danišik, M., Gjerazi, I., et al. (2021). The connection between the Alps and the Carpathians beneath the Pannonian basin: Selective reactivation of Alpine nappe contacts during Miocene extension. *Global and Planetary Change*, 197, 103401. <https://doi.org/10.1016/j.gloplacha.2020.103401>
- Tari, G., & Horváth, F. (2010). Eo-alpine evolution of the Transdanubian range in the nappe system of the eastern Alps: Revival of a 15 years tectonic model (Hungarian with English abstract). *Földtani Közlemények*, 140(4), 483–510.
- Ustaszewski, K., & Schmid, S. M. (2006). Control of preexisting faults on geometry and kinematics in the northernmost part of the Jura fold-and-thrust belt. *Tectonics*, 25. <https://doi.org/10.1029/2005TC001915>
- Vörös, A., & Galácz, A. (1998). Jurassic palaeogeography of the Transdanubian central range (Hungary). *Rivista Italiana di Paleontologia e Stratigrafia*, 104(1), 69–84.
- Williams, G. D., Powell, C. M., & Cooper, M. (1989). Geometry and kinematics of inversion tectonics. *Geological Society of London Special Publications*, 44, 3–15. <https://doi.org/10.1144/gsl.sp.1989.044.01.02>
- Yagupsky, D. L., Cristallini, E. O., Fantín, J., Valcarce, G. Z., Bottesi, G., & Varadé, R. (2008). Oblique half-graben inversion of the Mesozoic Neuquén rift in the Malargüe fold and thrust belt, Mendoza, Argentina: New insights from analogue models. *Journal of Structural Geology*, 30(7), 839–853. <https://doi.org/10.1016/j.jsg.2008.03.007>